



HAL
open science

Influence of an initial incidence angle on the dynamics of inverted flags

Mohammad Tavallaeinejad, Michael Païdoussis, Mathias Legrand, Mojtaba Kheiri

► **To cite this version:**

Mohammad Tavallaeinejad, Michael Païdoussis, Mathias Legrand, Mojtaba Kheiri. Influence of an initial incidence angle on the dynamics of inverted flags. 27th Canadian Congress of Applied Mechanics, May 2019, Sherbrooke, Canada. hal-02151372

HAL Id: hal-02151372

<https://hal.science/hal-02151372>

Submitted on 8 Jun 2019

HAL is a multi-disciplinary open access archive for the deposit and dissemination of scientific research documents, whether they are published or not. The documents may come from teaching and research institutions in France or abroad, or from public or private research centers.

L'archive ouverte pluridisciplinaire **HAL**, est destinée au dépôt et à la diffusion de documents scientifiques de niveau recherche, publiés ou non, émanant des établissements d'enseignement et de recherche français ou étrangers, des laboratoires publics ou privés.

INFLUENCE OF AN INITIAL INCIDENCE ANGLE ON THE DYNAMICS OF INVERTED FLAGS

Mohammad Tavallaeinejad, Michael P. Païdoussis,
 Mathias Legrand
 Mechanical Engineering
 McGill University
 Montreal, Quebec, Canada
 mohammad.tavallaeinejad@mail.mcgill.ca

Mojtaba Kheiri
 Mechanical,
 Industrial and Aerospace Engineering
 Concordia University
 Montreal, Quebec, Canada

ABSTRACT

A nonlinear fluid-elastic model is developed in order to study the dynamics of two-dimensional inverted flags subject to wind at an initial angle of attack. Theodorsen's quasi-steady aerodynamic theory is used for the inviscid fluid-dynamic modelling of the deforming flag. The Polhamus leading edge suction analogy is employed to model flow separation effects from the free end at moderate angles of attack via a nonlinear vortex-lift force. The flag dynamics is solely described by the angle of rotation within the geometrically-exact Euler-Bernoulli beam theory. The equation of motion is discretised spatially via the Galerkin method. Bifurcation diagrams are obtained using a pseudo-arclength continuation technique. The numerical results show that inverted flags undergo multiple bifurcations as the flow velocity is increased. It is shown that transition between the regimes occurs at flow velocities inversely proportional to the initial incidence angle. It is also shown that, for sufficiently large mass ratios, the existence of a strong subcritical periodic solution can lead to direct transition from the stretch-straight (undeflected) state to large-amplitude flapping motion.

Keywords: Inverted flag, Fluid-Structure Interaction, Nonlinear dynamics

INTRODUCTION

The dynamics of a subset of fluid-structure interaction (FSI) problems involving a cantilevered flexible thin plate (also termed a flag) subjected to a fluid flowing axially from the free end towards the clamped one, otherwise known as an 'inverted flag', has attracted attention due to its engineering applications, such as small scale energy harvesting systems [1, 2] and heat transfer enhancement in heat exchangers [3]. There has been ongoing research on this FSI problem over the past few years, aiming to understand the dynamics of the system [4, 5, 6, 7, 8].

It is of interest to explore the dynamical behaviour of inverted flags when they are subject to oncoming flow with a non-zero

angle of attack ψ_0 , as illustrated in Fig. 1. This problem is of

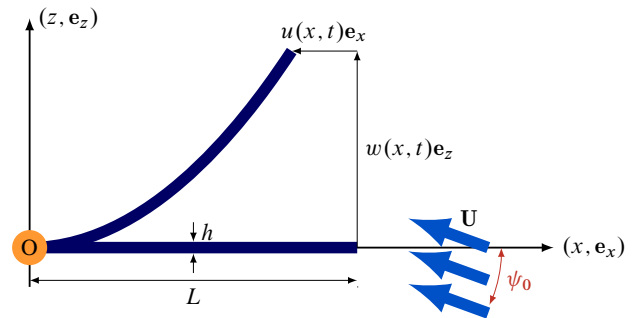


Figure 1: Idealised inverted flag in axial flow with a small initial angle of attack ψ_0

practical importance in the design of energy harvesters suitable for ambient wind conditions where the wind direction is not necessarily aligned with the flag neutral plane [1]. The effect of initial angle of attack has been investigated experimentally by Cossé et al. [9] and computationally by Shoele et al. [2] as well as Tang et al. [10]. The aim of the present paper is to derive an *analytical* model able to capture to explore the nonlinear dynamics and post-critical behaviour of inverted flags with an initial angle of attack.

ANALYTICAL MODELLING

The system under consideration is shown schematically in Fig. 1. It consists of a vertical cantilevered thin plate subjected to an inviscid axial flow impinging on its free end.

The flag is idealized as an Euler-Bernoulli beam, thus the spanwise deformation is neglected. The aerodynamic forces are modelled via a two-dimensional incompressible flow theory. The inverted flag is of chord L , thickness h , cross-sectional area A , flexural rigidity D , and transverse moment of inertia I . The mechanical properties of the flag, i.e., its mass density, Poisson

ratio, Young's modulus, and internal damping coefficient are represented by ρ_p , ν , E , and η , respectively; ρ_f denotes the density of the fluid flowing with mean flow velocity U . The neutral plane of the inverted flag is rotated by ψ_0 with respect to the direction of the undisturbed flow, noting that ψ_0 is constant with respect to temporal and spatial coordinates.

For an inextensible cantilevered beam, the rotation angle of a straight cross-section $\psi(x, t)$ ¹ as well as the curvature $\kappa(x, t)$ are related to the longitudinal, $u(x, t)$, and transverse, $w(x, t)$, motions of an arbitrary point located at a distance z from the mid-plane on the cross-section by $\sin \psi = \partial_x w$, $\cos \psi = 1 + \partial_x u$, and $\kappa = \partial_x \psi$, where ∂_x denotes the first spatial derivative. Consequently, w and u can be formulated in terms of the rotation angle of the cross-section ψ , as the primary variable for describing the flag motion. Derivation of the equation of motion in terms of the rotation angle allows prediction of large-amplitude deformations even when the tip rotation exceeds $\pi/2$ [8].

The projection of the undistributed flow velocity onto the x and z directions leads to $U_x = \mathbf{U} \cdot \mathbf{e}_x = U \cos \psi_0$ and $U_z = \mathbf{U} \cdot \mathbf{e}_z = U \sin \psi_0$, respectively. Consequently, the normal and tangential components of the relative flow velocity are given by

$$V_n(x, t) = (\dot{w} - U \sin \psi_0) \cos \psi - (\dot{u} + U \cos \psi_0) \sin \psi, \quad (1a)$$

$$V_\tau(x, t) = (\dot{u} + U \cos \psi_0) \cos \psi + (\dot{w} - U \sin \psi_0) \sin \psi, \quad (1b)$$

with overdot being differentiation with time. The inviscid pressure-related forces corresponding to the relative motion of the inverted flag and the incident flow are modelled based on the two-dimensional quasi-steady thin airfoil theory involving large angles of attack [11, 12]. First, the quasi-steady forces are derived using a velocity potential approach in a way that the solution is divided into non-circulatory and circulatory contributions, each part of which is conveniently obtained using Joukowski's conformal transformation. Next, the effects of separated flow at the leading edge are modelled by utilizing Polhamus's leading edge suction analogy [13]. Hence, the total normal force acting on the flag is formulated as

$$F_N(\theta, t) = -(\Delta P^{\text{nc}} + \Delta P^{\text{c}}) - 2F_p(t)\delta_D(\cos \theta - 1), \quad (2)$$

where

$$\Delta P^{\text{nc}}(\theta, t) = -\rho \left(\frac{L}{2} \partial_t \left[\int_\theta^0 \int_0^\pi \frac{V_n(\varphi, t) \sin^2 \varphi}{\cos \varphi - \cos \vartheta} d\varphi d\vartheta \right] - \frac{(\dot{u} + U) \cos \psi + \dot{w} \sin \psi}{\sin \theta} \int_0^\pi \frac{V_n(\varphi, t) \sin^2 \varphi}{\cos \varphi - \cos \theta} d\varphi \right), \quad (3)$$

$$\Delta P^{\text{c}}(\theta, t) = -\frac{\rho V_\tau}{\sin \theta} \frac{2}{\pi} \int_0^\pi V_n(\varphi, t) (1 - \cos \varphi) d\varphi, \quad (4)$$

$$F_p(t) = \frac{\rho_f L}{16\pi} \int_0^\pi V_d(\varphi, t) d\varphi \left| \int_0^\pi V_d(\varphi, t) d\varphi \right|, \quad (5)$$

in which $x = (1 + \cos \theta)/2$, $V_d(\varphi, t) = V_n(\varphi, t)(1 + \cos \varphi)$ and δ_D represents the Dirac delta distribution and is used to transfer the end-shear from the boundary condition into the equation of

¹It should be noted that the space and time dependencies are indicated only once when quantities of interest are introduced and when they cannot be omitted.

motion, in order to be able to discretize the equation of motion by the Galerkin method. The absolute operator is also used to modify the force so as to be always aligned with motion.

The singular integral in Eq. (3) is evaluated using Glauert's principal value integral given as

$$\frac{1}{\pi} \int_0^\pi \frac{\cos n\varphi}{\cos \varphi - \cos \theta} d\varphi = \frac{\sin n\theta}{\sin \theta}, \quad n = 0, 1, 2, \dots \quad (6)$$

To this end, the normal component of the relative velocity is expressed in a succession Taylor's expansions. This results in a polynomial representation of the induced velocity in terms of ψ . In this paper, third order Taylor's series expansions are retained.

Utilizing the dimensionless parameters $x^* = x/L$, $t^* = t/\tau$, $\beta = I/AL^2$, $\eta_d = \eta/\tau$, $f^* = f\tau$, $\mu = \rho_f L/(\rho_p h)$, $\Pi = \sqrt{\rho_f L/DLU}$, with f being the frequency of flapping and $\tau = \sqrt{\rho_p h/DL^2}$, the time scale, the equation of motion in terms of the rotation angle ψ can be expressed as

$$\begin{aligned} & \beta \ddot{\psi} - \eta_s \partial_{xx} \dot{\psi} - \partial_{xx} \psi \\ & - \sin \psi \partial_{tt} \left(\int_x^1 \int_0^s \cos \psi(\xi, t) d\xi ds \right) \\ & + \cos \psi \partial_{tt} \left(\int_x^1 \int_0^s \sin \psi(\xi, t) d\xi ds \right) \\ & + \cos \psi \int_1^x F_N^*(s, t) \cos \psi(s, t) ds \\ & + \sin \psi \int_1^x F_N^*(s, t) \sin(s, t) \psi ds = 0, \end{aligned} \quad (7)$$

where ∂_{tt} and ∂_{xx} represent the second differentiation with respect to time and space, respectively; F_N^* denotes the dimensionless counterpart of F_N . Note that the asterisk notation is dropped throughout for simplicity.

The clamped-free boundary conditions which read as $\psi(0, t) = 0$ and $\psi_x(L, t) = 0$.

The spatial discretisation of the nonlinear equation (7) is made through the Galerkin method, where a linear set of comparison functions $\Psi_i(x)$ is selected to approximate the rotation of the flag. Hence, $\psi(x, t) = \sum_{i=1}^M \Psi_i(x) q_i(t)$ where $q_i(t)$ are the unknown time-dependent generalized coordinates and M denotes the number of modes used.

NUMERICAL RESULTS

In this paper, $M = 6$ modes are employed to discretize Eq. (7) together with the following parameters: $L = 10$ cm, $h = 1$ mm, $\rho_p = 1200$ kg m⁻³, $\rho_f = 1.2$ kg m⁻³, $D = 2454$ N cm² and $\eta = 0.0002$. The dimensionless flow velocity Π is selected as the bifurcation parameter to explore the system dynamics.

The nonlinear response of the two-dimensional flag with $\mu = 0.1$, and $\psi_0 = 0.1 \approx 5.7^\circ$ is shown in Fig. 2. Even such a seemingly small angle of attack gives rise to asymmetric fluid loading on the inverted flag which consequently breaks the symmetry of the nonlinear response. More specifically, as opposed to the case with $\psi_0 = 0$, i.e. an inverted flag perfectly

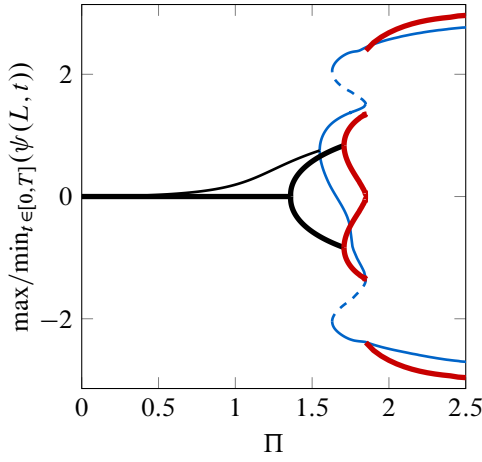


Figure 2: Bifurcation diagrams for two-dimensional inverted flags with $\mu = 0.1$ and (i) $\psi_0 = 0$ (heavy lines), for (ii) $\psi_0 = 0.1$, where the peak values of the leading edge rotation over a cycle of steady-state oscillation of period T^* are plotted as a function of Π . [—] Stable static solution; [---] unstable periodic solution; [—] stable symmetric periodic solution; and [—] stable periodic solution (asymmetric oscillations).

aligned with the incident flow (drawn with heavy lines), the flag bends continuously with increasing flow velocity (a gradual transition from small to large deflections). This behaviour is followed by a Païdoussis-type Hopf bifurcation at $\Pi = 1.55$ giving rise to a stable limit cycle corresponding to asymmetric flapping around the deflected equilibrium. This solution folds at the first saddle-node bifurcation encountered (at $\Pi = 1.84$) and becomes unstable. By tracing the unstable solution, a second saddle-node bifurcation arises at $\Pi = 1.63$ where the response of the system folds once again. Following the second saddle-node bifurcation, the solution becomes stable again, which is physically manifested as asymmetric large-amplitude flapping around the origin.

The bifurcation diagrams shown in Fig. 3 for $\psi_0 = 0.2$ examine the response of the system for different values of mass ratio μ . Different scenarios can be expected for flags of different mass ratios. While the sequence of progressive bending to asymmetric deformed-flapping to asymmetric large-amplitude flapping is more plausible for the inverted flag with a low mass ratio, e.g. $\mu = 0.1$, the flag with the high mass ratio of $\mu = 5.0$, if sufficiently perturbed, may turn directly from the buckled shape to large-amplitude flapping due to the presence of a limit cycle in the fairly close of the static solution.

The sensitivity of the nonlinear response of the system to ψ_0 is shown in Fig. 4. The numerical results show fairly good agreement with observations by Cossé et al. [9], who investigated experimentally the effects of flag orientation to the impinging flow on the dynamics of the system. For example, Cossé et al. [9] reported that the transition between bifurcations for $\psi_0 \neq 0$ was gradual, as opposed to the case with $\psi_0 = 0$, where an abrupt jump to large-amplitude flapping was observed. This agrees well with the present results which show that the transition be-

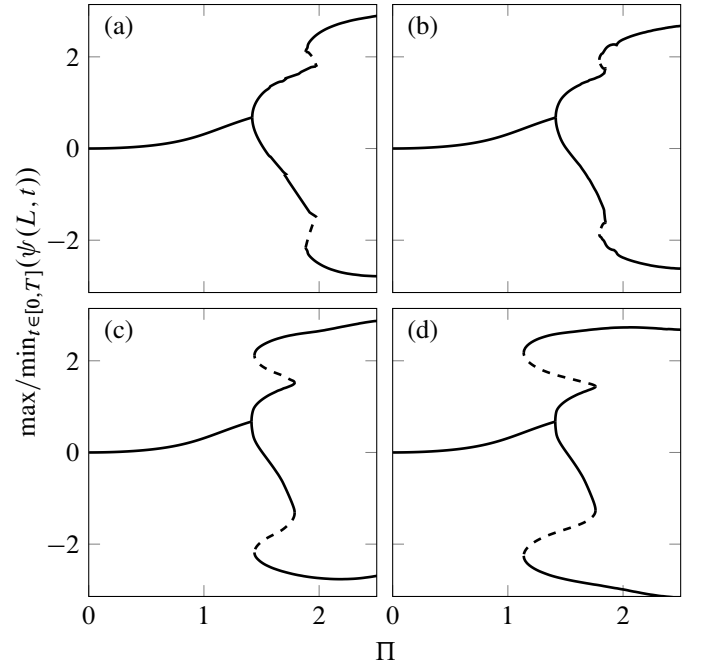


Figure 3: Bifurcation diagrams for two-dimensional inverted flags with $\psi_0 = 0.2$, and various mass ratios: (a) $\mu = 0.1$, (b) $\mu = 0.5$, (c) $\mu = 2.0$ and (d) $\mu = 5.0$.

tween the two flapping motions becomes smoother as ψ_0 is increased. Furthermore, as seen in Fig. 4, varying ψ_0 affects the onset of flapping significantly: for inverted flags with larger initial angle of attack, the asymmetric flapping motion around the buckled shape occurs at lower flow velocities. The amplitude of large-amplitude flapping also decreases correspondingly. These also agree well with the measurements reported in [9], which reveal that, as the initial angle of attack is increased, the transition from static equilibrium to the flapping mode occurs at lower flow velocities and with smaller amplitude of oscillations. Moreover, as seen in Fig. 4 for all investigated cases, the inverted flag undergoes asymmetric deformed-flapping motion at different critical flow velocities, which is consistent with the computational findings by Shoele et al. [2, 10] and, again, the experimental observations in [9].

CONCLUSION

An analytical model was proposed to explore the nonlinear dynamics of two-dimensional inverted flags subject to wind at an initial angle of attack ψ_0 . The nonlinear partial-integro-differential equation governing the dynamics of the inverted flag in terms of the angle of rotation was discretised, using the Galerkin technique, and then the resulting nonlinear ODEs were solved via a pseudo-arclength scheme to construct bifurcation diagrams. It was shown that the transition between the two flapping motions becomes smoother as ψ_0 increases. Moreover, the sensitivity of the onset of flapping to ψ_0 is high. For inverted flags with large ψ_0 , the asymmetric flapping motion around the buckled shape occurs at low flow velocities. These findings

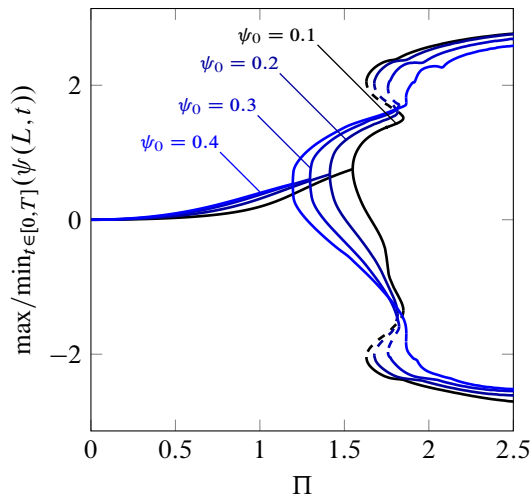


Figure 4: Bifurcation diagram for the investigated inverted flag with $\mu = 1.0$ and various initial angles of attack ψ_0 .

highlight the ability of inverted flags to perform flapping motion even when the oncoming flow is not parallel to their longitudinal axis. The outcome can be of practical importance for the design of robust energy harvesters in actual ambient conditions.

ACKNOWLEDGMENT

The authors gratefully acknowledge the financial support by the Natural Sciences and Engineering Research Council of Canada, the Solution Mining Research Institute (SMRI) and Pipeline Research Council International (PRCI). The last author also appreciates the financial support by Concordia University through a Start-Up grant.

REFERENCES

- [1] Orrego, S., Shoele, K., Ruas, A., Doran, K., Caggiano, B., Mittal, R., and Kang, S. H., 2017. “Harvesting ambient wind energy with an inverted piezoelectric flag”. *Applied Energy*, **194**, pp. 212–222. [10.1016/j.apenergy.2017.03.016](https://doi.org/10.1016/j.apenergy.2017.03.016).
- [2] Shoele, K., and Mittal, R., 2016. “Energy harvesting by flow-induced flutter in a simple model of an inverted piezoelectric flag”. *Journal of Fluid Mechanics*, **790**, pp. 582–606. [10.1017/jfm.2016.40](https://doi.org/10.1017/jfm.2016.40).
- [3] Park, S. G., Kim, B., Chang, C. B., Ryu, J., and Sung, H. J., 2016. “Enhancement of heat transfer by a self-oscillating inverted flag in a poiseuille channel flow”. *International Journal of Heat and Mass Transfer*, **96**, pp. 362–370. [10.1016/j.ijheatmasstransfer.2016.01.043](https://doi.org/10.1016/j.ijheatmasstransfer.2016.01.043).
- [4] Kim, D., Cossé, J., Huertas Cerdeira, C., and Gharib, M., 2013. “Flapping dynamics of an inverted flag”. *Journal of Fluid Mechanics*, **736**. [hal-02005035](https://doi.org/10.1017/jfm.2013.139).
- [5] Sader, J., Cossé, J., Kim, D., Fan, B., and Gharib, M., 2016. “Large-amplitude flapping of an inverted flag in a uniform

steady flow—a vortex-induced vibration”. *Journal of Fluid Mechanics*, **793**, pp. 524–555. [10.1017/jfm.2016.139](https://doi.org/10.1017/jfm.2016.139).

- [6] Sader, J., Huertas-Cerdeira, C., and Gharib, M., 2016. “Stability of slender inverted flags and rods in uniform steady flow”. *Journal of Fluid Mechanics*, **809**, pp. 873–894. [10.1017/jfm.2016.691](https://doi.org/10.1017/jfm.2016.691).
- [7] Tavallaeinejad, M., Legrand, M., and Païdoussis, M. “Non-linear response of inverted flags subjected to a steady flow”. In 9th International Symposium on Fluid-Structure Interactions, Flow-Sound Interactions, Flow-Induced Vibration & Noise, July 8-11, 2018, Toronto, Canada. [hal-01812870](https://doi.org/10.1115/PVP2018-91187).
- [8] Tavallaeinejad, M., Païdoussis, M., and Legrand, M., 2018. “Nonlinear static response of low-aspect-ratio inverted flags subjected to a steady flow”. *Journal of Fluids and Structures*, **83**, pp. 413–428. [hal-01745147](https://doi.org/10.1016/j.jfs.2018.03.017).
- [9] Cossé, J., Sader, J., Kim, D., Cerdeira, C. H., and Gharib, M. “The effect of aspect ratio and angle of attack on the transition regions of the inverted flag instability”. In ASME Pressure Vessels and Piping Conference, July 20-24, 2014, Anaheim, USA. [10.1115/PVP2014-28445](https://doi.org/10.1115/PVP2014-28445).
- [10] Tang, C., Liu, N.-S., and Lu, X.-Y., 2015. “Dynamics of an inverted flexible plate in a uniform flow”. *Physics of Fluids*, **27**(7). [10.1063/1.4923281](https://doi.org/10.1063/1.4923281).
- [11] Bisplinghoff, R., Ashley, H., and Halfman, R., 2013. *Aeroelasticity*. Courier Corporation.
- [12] Yan, Z., Taha, H., and Hajj, M., 2014. “Geometrically-exact unsteady model for airfoils undergoing large amplitude maneuvers”. *Aerospace Science and Technology*, **39**, pp. 293–306. [10.1016/j.ast.2014.09.021](https://doi.org/10.1016/j.ast.2014.09.021).
- [13] Polhamus, E., 1966. A concept of the vortex lift of sharp-edge delta wings based on a leading-edge-suction analogy. Tech. rep., NASA. [19670003842](https://doi.org/10.1016/j.jfm.2016.139).